A humanised tissue-engineered bone model allows species-specific breast cancer-related bone metastasis *in vivo*

Quent VMC [1], Taubenberger AV [2], Reichert JC [3], Martine LC [4], Clements JA [4,5], Hutmacher DW [4,5,6,7]* and Loessner D [4,8]*

[1] Department of Obstetrics and Gynecology, Martin-Luther-Krankenhaus, Academic Teaching Hospital of the Charité Berlin, Caspar-Theyß-Str. 27-31, 14193 Berlin, Germany;
[2] Biotechnology Center Dresden, Technical University of Dresden, Am Tatzberg 47-49, 01307 Dresden, Germany;
[3] Department of Orthopedics and Accident Surgery, Waldkrankenhaus Protestant Hospital, Academic Teaching Hospital of the Charité Berlin, Stadtrandstr. 555, 13589 Berlin, Germany;
[4] Queensland University of Technology (QUT), 60 Musk Avenue, Kelvin Grove, QLD 4059, Brisbane, Australia;
[5] Australian Prostate Cancer Research Centre - Queensland, Translational Research Institute, Queensland University of Technology, 37 Kent Str, Woolloongabba, QLD 4102, Brisbane, Australia;
[6] George W Woodruff School of Mechanical Engineering, Georgia Institute of Technology, 801 Ferst Drive Northwest, Atlanta, GA 30332, US;
[7] Institute for Advanced Study, Technische Universität München, Lichtenbergstr. 2a, 85748 Garching, Germany;
[8] Barts Cancer Institute, Queen Mary University of London, Charterhouse Square, EC1M 6BQ London, United Kingdom.

*__Corresponding authors:__

Prof Dietmar W Hutmacher
Chair of Regenerative Medicine
Institute of Health and Biomedical Innovation
Centre in Regenerative Medicine
Queensland University of Technology
60 Musk Ave, Kelvin Grove, QLD 4059
Phone: +61 7 3138 6077
Fax: +61 7 3138 6030
Email: dietmar.hutmacher@qut.edu.au

Dr Daniela Loessner
Centre for Regenerative Medicine

+61 7 3138 6441
+61 7 3138 6030
daniela.lossner@qut.edu.au

This article has been accepted for publication and undergone full peer review but has not been through the copyediting, typesetting, pagination and proofreading process which may lead to differences between this version and the Version of Record. Please cite this article as doi: 10.1002/term.2517

Abstract

Bone metastases frequently occur in the advanced stages of breast cancer. At this stage, the disease is deemed incurable. To date, the mechanisms of breast cancer-related metastasis to bone are poorly understood. This may be attributed to the lack of appropriate animal models to investigate the complex cancer cell-bone interactions. In this study, two established tissue-engineered bone constructs (TEBCs) were applied to a breast cancer-related metastasis model. A cylindrical medical-grade polycaprolactone-tricalcium phosphate scaffold produced by fused deposition modelling (scaffold 1) was compared with a tubular calcium phosphate-coated polycaprolactone scaffold fabricated by solution electrospinning (scaffold 2) for their potential to generate ectopic humanised bone in NOD/SCID mice. While the scaffold 1 was found not suitable to generate a sufficient amount of ectopic bone tissue due to poor ectopic integration, the scaffold 2 showed excellent integration into the host tissue, which did lead to bone formation. To mimic breast cancer cell colonisation to the bone, MDA-MB-231, SUM1315 and MDA-MB-231BO breast cancer cells were cultured in polyethylene glycol-based hydrogels and implanted adjacent to the TEBCs. Histological analysis indicated that the breast cancer cells induced an osteoclastic reaction in the TEBCs, demonstrating analogies to breast cancer-related bone metastasis seen in patients.

Keywords: bone tissue engineering, breast cancer, polycaprolactone scaffolds, fused deposition modelling, solution electrospinning, humanised animal model, bone colonisation

1. Introduction

Breast cancer is the most common malignancy in women according to the WHO, and over half a million women died from this disease in 2011 (DeSantis *et al.* 2011). Survival rates vary from 80% for example in North America, Sweden and Japan to approximately 40-60% in middle-income and low-income countries (Coleman M. P. *et al.* 2008). This wide range might be due to inadequate treatment, lack of early detection and poor diagnostic tools, thus women are diagnosed with the advanced stage of the disease (Coleman M. P. *et al.* 2008). Despite the availability of well-established treatment modalities, including surgery, chemo-, radiation- and anti-hormonal therapy, and therefore high survival rates in high-income countries, at least 10-15% of breast cancer patients develop metastases after years of disease-free survival (Coleman R. E. and Rubens 1987) (Psaila *et al.* 2006). Breast cancer-related metastases mainly affect the skeleton followed by the liver, lung and brain (Coleman R. E. and Rubens 1987) (Kozlow and Guise 2005). The skeleton represents the major tissue

for breast cancer metastases, about 83% of women with advanced disease suffer from this debilitating stage.

Bone metastases are classified according to their radiographic appearance as osteolytic or osteoblastic (Thibaudeau *et al.* 2014a). Both types of bone lesions are caused by an imbalance between bone resorption through activated osteoclasts and new bone formation through osteoblasts. Osteolytic lesions show a deficient new bone formation, while osteoblastic lesions have a disorganised new bone formation with impaired bone resorption (Thibaudeau *et al.* 2014a). Osteolytic lesions are predominant in breast cancer-related bone metastasis (Yu *et al.* 2012). Symptoms associated with bone metastases are due to extensive bone loss and tumour expansion, and include severe bone pain, pathological fractures, spinal cord compression and hypercalcaemia (Kozlow and Guise 2005) (Yu *et al.* 2012). Current treatment options for bone metastasis are seldom curative and focus on pain management (Thibaudeau *et al.* 2014a). The frequency of pathological fractures can be decreased through palliative treatment with anti-resorptive drugs like bisphosphonates and the RANKL antibody denosumab (Thibaudeau *et al.* 2014a). These treatments improve the quality of life, but fail to prolong patient survival (Daniele *et al.* 2011) (Brown *et al.* 2004).

The restricted treatment options are due to the fact that underlying mechanisms of breast cancer-related bone metastasis are not fully understood which in turn results from the lack of appropriate *in vitro* and *in vivo* models to study this disease. Current *in vivo* approaches investigate the homing of human breast cancer cells to the murine skeleton in immune-compromised hosts. These models present two disadvantages. Firstly, injection of cancer cells into the murine circulatory system via tail vein or left ventricle bypasses the first steps of the metastatic cascade (Kang *et al.* 2003). Secondly, interspecies phenomena are examined as human breast cancer cells interact with the murine bone. Yonou *et al*. (Yonou *et al.* 2001) were the first to use adult human bone fragments as metastatic target for osteotropic cancer cells as opposed to the murine skeleton. However, the route of cancer cell injection remained the same (Lau *et al.* 2013) (Khanna and Hunter 2005). Other models utilised cell carrier systems, such as Matrigel or other hydrogels, to induce a human breast tumour at its orthotopic site, the murine mammary fat pad, to recapitulate the metastatic cascade but failed to generate a bone marrow compartment (Kuperwasser *et al.* 2005). Since then, only a few models used human bone fragments in conjunction with orthotopic breast tumours (Xia *et al.* 2012). However, these models are linked with partial necrosis of the bone fragments due to delayed neo-vascularisation, high variability and donor dependency, resulting in poor reproducibility (Moreau *et al.* 2007). A strategy to overcome these complications has been the introduction of a bone tissue engineering (TE) approach (Thibaudeau *et al.* 2014a) (Thibaudeau *et al.* 2014b) (Schuster *et al.* 2006) (Bersani *et al.* 2014) (Seib *et al.* 2015).

Scaffolds for the purpose of bone TE need to have a high elastic modulus and an interconnected macro-pore structure of 300-500 µm to enhance diffusion rates to and from the scaffold centre and to allow the transport of nutrients and by-products (Hutmacher 2000). Medical-grade polycaprolactone-tricalcium phosphate (mPCL-TCP) scaffolds produced by fused deposition modelling meet the aforementioned requirements (Hutmacher 2000). Composite scaffolds represent a combination of bioactive ceramics, such as calcium phosphate (CaP), with a polymer, such as mPCL, to combine the favourable mechanical properties of the biodegradable polymer with the osteoconductive characteristics of the ceramic component (Zhou *et al.* 2007). Previously, mPCL-TCP scaffolds have been used in rat and rabbit skull defect models as well as in a spinal fusion model with promising outcomes (Hutmacher and Cool 2007). To further improve the osteoinductivity of these bone TE approaches, scaffolds have been used in conjunction with osteogenic progenitor cells and growth factors like bone morphogenetic proteins (BMPs) (Arthur *et al.* 2009) (Biggs *et al.* 2009) (Santos *et al.* 2009).

This study shows the attempt to translate an orthotopic bone TE approach to an ectopic humanised NOD/SCID model. This approach has already been successfully used by our group to mimic the invasion of the humanised bone by breast cancer cells upon intra-cardiac injection (Thibaudeau *et al.* 2014a) (Thibaudeau *et al.* 2014b). Herein, the development of a model of direct bone colonisation, by implanting cell-loaded hydrogels adjacent to the tissue-engineered bone constructs (TEBCs), opposed to the experimental or spontaneous metastasis approach, is described. Therefore, two TEBCs with different architectures and manufacturing techniques were compared.

2. Materials and Methods

2.1. Isolation of human osteoblasts

Primary human osteoblasts (hOBs) were isolated from explants obtained from patients undergoing knee replacement surgery as approved by the Queensland University of Technology and Prince Charles Hospital ethics committees (approval number 0600000232). Non-sclerotic, trabecular bone from the tibial plateau was collected, minced, washed and transferred into tissue culture flasks containing α-Minimal Essential Medium (α-MEM), 10% FBS, penicillin (100 IU/ml) and streptomycin (0.1 mg/ml).

2.2. Cell lines

MCF10A (non-malignant and non-invasive) and MDA-MB-231 (highly invasive and metastatic) cells were purchased from the American Type Culture Collection. SUM1315 cells

(invasive) were kindly provided by Prof David Kaplan (Tufts University, US). MDA-MB-231BO cells (highly invasive) characteristically prone to develop bone metastasis were provided by The University of Texas Health Science Center at San Antonio. MCF10A cells were cultured in Dulbecco's Modified Eagle Medium (DMEM)/F-12, EGF (20 ng/ml), insulin (0.01 mg/ml) and cholera toxin (100 ng/ml). SUM1315 cells were cultured in DMEM/F-12, EGF (10 ng/ml) and insulin (5 µg/ml). MDA-MB-231 and MDA-MB-231-BO cells were maintained in DMEM. Each medium contained 10% FBS, penicillin (100 IU/ml) and streptomycin (0.1 mg/ml).

2.3. Scaffold fabrication using fused deposition modelling (scaffold 1)

Composite mPCL-TCP scaffolds were produced by fused deposition modelling (Osteopore International, Singapore). Composite scaffold sheets (mPCL:TCP, 80:20) measuring 100×100×4 mm, with a lay down pattern of 0/60/120º, 100% pore interconnectivity, 380-500 µm pore size and 70% porosity, were produced as described previously (Zhou *et al.* 2007). Biopsy punches were used to produce cylindrical scaffolds of 4 mm height, with an outer diameter of 8 mm and an inner diameter of 4 mm (Fig. 1A-D). Scaffolds were treated with 1 M NaOH for 6 hrs to hydrolytically cleave mPCL chains and transform ester groups into carboxy and hydroxyl groups for increased hydrophilicity. Then, scaffolds were washed with PBS and 70% ethanol, followed by evaporation and UV sterilisation for 30 min. Further characterisation was performed as reported previously (Reichert *et al.* 2011).

2.4. Scaffold fabrication using solution electrospinning (scaffold 2)

Solution electrospun-fabricated mPCL scaffolds were a generous gift from Prof Robert Guldberg (George W Woodruff School of Mechanical Engineering, Georgia Institute of Technology, US). Characterisation was carried out in the Guldberg group as reported previously (Kolambkar *et al.* 2011). Briefly, to obtain tubular scaffolds, nanometre-sized sheets were cut into 13×19 mm rectangular shapes, perforated 1.5 mm apart using a 1 mm biopsy punch and wrapped around a steel mandrel to form a tube of 5 mm diameter. Overlapping edges were aligned with UV glue (Fig. 1E-F). The fibre diameter was quantified using scanning electron microscopy and a custom MATLAB® program. Fibre diameter ranged from 51-974 nm, with 82% of the fibres between 50-150 nm. Scaffolds were 300-400 µm thick, with 80-90% porosity and had a pore size of less than 5 µm (Fig. 1G). Sterilisation was performed as above.

2.5. CaP coating of solution electrospun-fabricated scaffolds

Scaffolds were immersed in 70% ethanol for 30 min under vacuum and treated with 37°C pre-warmed 2 M NaOH for 5 min under vacuum, facilitating solution penetration through the entire scaffold to enhance the efficacy of alkaline etching. Then, scaffolds were rinsed with ddH_2O to neutralise the pH. Simulated Body Fluid (SBF-10x) was prepared and filtered (filter pore size 0.2 µm) as reported previously (Yang *et al.* 2008), with pH 6 to increase the solution stability and delay CaP precipitation. A 5 min vacuum treatment was performed to enable SBF infiltration into the scaffolds, followed by 2.5 hrs SBF incubation at 37°C, with SBF changes every 30 min. A 0.5 M NaOH post-treatment for 30 min at 37°C obtained a homogenous CaP coating. Then, scaffolds were rinsed with ddH_2O, air-dried and placed into a desiccator until usage. To evaluate the distribution of the CaP coating, micro-computed tomography (µ-CT) analysis, with a 12 µm voxel size, at 45 kV and 177 µA was performed. Following parameters were applied: a threshold of 100 Hounsfield Units, a filter width of 0.8 and filter support of 1.0. Three-dimensional reconstructions were obtained using the software package supplied by Scanco Medical AG (Vaquette *et al.* 2013).

2.6. Cell seeding of scaffolds

Sterile mPCL-TCP and mPCL-CaP scaffolds were placed into a 24-well plate, and 1.5×10^5 hOBs in 50 µl medium were equally distributed onto the scaffolds and incubated at 37ºC/5% CO_2 to allow cell adhesion. After 2 h, 1 ml of medium was carefully added. Cells were cultured in osteogenic medium, containing L-ascorbic acid 2-phosphate (50 µg/ml), β-glycerophosphate (10 mM) and dexamethasone (0.1 µM) over 4 weeks with medium changes twice per week.

2.7. Live/dead assay

After 4 weeks of 3D culture, a live/dead assay was performed using fluorescein diacetate (FDA) and propidium iodide (PI) staining. Samples were rinsed with 37°C pre-warmed phenol red-free medium and incubated with FDA (2 µg/ml) and PI (20 µg/ml) staining solution prepared in medium at 37ºC/5% CO_2 for 15 min. Then, samples were washed in PBS, containing $CaCl_2$ (0.901 mM) and $MgCl_2\times6H_2O$ (0.493 mM), and imaged using a Leica SP5 laser scanning confocal microscope.

2.8. Assessment of cell morphology

After 4 weeks of 3D culture, samples were fixed with 4% PFA/PBS for 20 min and permeabilised with 0.2% Triton X-100/PBS for 5 min at room temperature. Then, samples were washed in PBS and blocked in 2% BSA/PBS for 20 min, followed by incubation with

PicoGreen™ (1:1,000) and rhodamine415-conjugated phalloidin (0.3 U/ml) staining solution in 2% BSA/PBS for 1 h. DAPI (2.5 µg/ml) staining was used to visualise cell nuclei. Samples were washed in PBS to remove any residual staining solution and immersed in PBS and imaged using a Leica SP5 laser scanning confocal microscope.

2.9. Implantation of the TEBCs

Animal experiments were conducted as approved by the Queensland University of Technology animal ethics committee (approval number 0900000915). Pre-seeded scaffolds were transplanted into the left and right flank by preparing subcutaneous pockets at the dorsal site of anaesthetised (25 mg/ml xylazine, 50 mg/ml ketamin, 9-10 µl/g body weight i.p.) 7-week old female NOD/SCID mice (ARC, Australia; 3 mice/group). To administer rhBMP-7 (10 µg/scaffold; Olympus Biotech, US) and additional hOBs (8×10^5/scaffold), 110 µl of fibrin sealant (Tisseel; Baxter, US) was applied to the inner duct of the scaffold intraoperatively (Fig. 2). Twelve weeks post-implantation, scaffolds were explanted for subsequent analyses.

2.10. Implantation of human non-malignant and malignant breast cell-loaded hydrogels

Polyethylene glycol (PEG)-based hydrogels were prepared as described previously (Loessner *et al.* 2010) and implanted under general anaesthesia adjacent to the TEBCs. Briefly, a 5% PEG-Gln/PEG-MMP-Lys precursor stock solution was diluted to the desired PEG concentration in Tris-buffered saline (50 mM, pH 7.6) containing RGD peptide (50 µM) and $CaCl_2$ (50 mM). Immediately after adding thrombin-activated factor XIII (10.7 U/ml), the breast cancer cell suspension was added (3.5×10^5 cells/ml). Cell-loaded hydrogel discs were formed by sandwiching 25 µl of the reaction mixture between two sterile glass slides, separated by 1.5 mm spacers and pre-coated with Sigmacote®, for 30 min at 37ºC/5% CO_2 to allow polymerisation. Then, hydrogels were transferred into 24-well plates and cultured for 3 days prior to implantation. Additionally, triplicate samples per cell line were cultured for 14 days to assess cell upon 3D culture. Four weeks post-implantation of cell-loaded hydrogels, animals were euthanised, scaffolds retrieved and fixed in 4% PFA for 24 hrs followed by 2% PFA for 48 hrs and stored in 70% ethanol for subsequent analysis. Tumour tissues were explanted and the tumour dimensions measured with a vernier calliper.

2.11. Micro-CT analysis

Samples were scanned with a 16 µm voxel size at 55 kV and 145 µA. Following parameters were applied: a threshold of 140 Hounsfield Units, a filter width of 1.0 and filter support of 2.0. X-ray attenuation was correlated to sample density using a standard curve generated by

scanning hydroxyapatite phantoms with known mineral density. Three-dimensional reconstructions were obtained using the software package supplied by Scanco Medical AG (Vaquette *et al.* 2013), and the bone volume (BV) and total volume (TV) fractions were quantified.

2.12. Immunohistochemistry

Samples were treated with 10% EDTA for at least 10 days to assure sufficient decalcification prior to paraffin embedding and serial sectioning (5 µm) using standard procedures. Samples were stained with Mayer's haematoxylin and eosin (H&E), human-specific antibodies (Table 1) and visualised using a Zeiss Axio Imager A.1 with an AxioCam MRc Rev 3 digital camera.

2.13. Tartrate resistant acid phosphatase (TRAP) staining and quantification of osteoclast numbers

To detect osteoclasts, TRAP staining was performed as described previously (Thibaudeau *et al.* 2014b). Briefly, deparaffinised sections were treated with 0.2 M acetate buffer (0.2 M sodium acetate, 50 mM L(+) tartaric acid in ddH_2O, pH 5.0) for 20 min at room temperature. Then, samples were incubated with naphtol AS-MX phosphate (0.5 mg/ml) and fast red TR salt (1.1 mg/ml) in 0.2 M acetate buffer for up to 4 hrs at 37ºC until osteoclasts appeared bright red. Samples were counterstained with Mayer's haematoxylin and visualised using a Zeiss Axio Imager A.1 with an AxioCam MRc Rev 3 digital camera. The number of osteoclasts was determined using the ImageJ software (NIH). For each group, 16 images representing the total area of new bone formation, taken at two different depths of the scaffold, were analysed. The number of osteoclasts was counted and normalised to the length of the respective bone line.

2.14. Statistical analysis

Datasets were tested for normality using SPSS software (IBM). Normally distributed data were then tested for statistical differences using a Student t-test or one-way ANOVA. $P<0.05$ was considered significant.

3. Results

3.1. Similar morphology and viability of hOBs grown on different scaffolds

Morphology and viability of hOBs was assessed after 4 weeks of 3D culture on both mPCL-TCP and mPCL-CaP scaffolds by bright-field (Suppl.Fig. 1A, D) and confocal microscopy (Suppl.Fig. 1B-C, E-F), revealing an elongated and spindle-shaped morphology of hOBs forming a dense, interconnected 3D network around the pores of both constructs. Cell viability was greater than 90% (Suppl.Fig. 1C, F).

3.2. Tubular mPCL-CaP scaffolds showed a superior incorporation into murine soft tissues

After 4 weeks of *in vitro* culture and osteogenic induction, hOB-seeded constructs were implanted into the flanks of female NOD/SCID mice. No adverse reaction was observed post-implantation of scaffolds, and scaffolds were well-tolerated over the duration of the experiments. Twelve weeks post-implantation, scaffolds were explanted. The delicate skin of NOD/SCID mice was not strong enough to aid the integration of the mPCL-TCP scaffold (scaffold 1; Suppl.Fig. 2A-D) in comparison to the mPCL-CaP scaffold (scaffold 2; Suppl.Fig. 2F) into the murine soft tissues due to its mechanical properties. Both TEBCs were well-vascularised at the time of explantation (Suppl.Fig. 2E, F). Micro-CT analysis showed that the mineralised tissue was distributed equally throughout both scaffolds and that the mPCL-TCP scaffold had a higher amount of mineralised tissue close to the muscle, but less mineralised tissue close to the skin (Fig. 3A, E). H&E staining revealed new bone (NB) formation and connective tissue (CT) in both scaffolds (Fig. 3B-C, F-G). TRAP staining indicated the presence of osteoclasts actively degrading the bone-like matrix in both scaffolds, with the mPCL-CaP scaffold group showing a higher amount of TRAP-positive cells (Fig. 3D, H). Although both scaffolds had equal osteoinductive properties, the mPCL-CaP scaffold (scaffold 2) was used for all subsequent experiments due to its better integrative and bone resorption features.

3.3. Distincitve cell morphologies of non-malignant and breast cancer cells grown within hydrogels

To assess the morphological differences of the all cell lines tested upon 3D cultures, cells were grown for 14 days within PEG-based hydrogels. Each cell line showed a distinct morphology within the hydrogels as visualised by immunofluorescent staining and confocal

laser scanning microscopy. Non-malignant MCF10A cells formed regular-shaped spheroids and a cell layer on top of the hydrogel (Suppl.Fig. 3A). SUM1315 cells formed only a few multicellular spheroids and remained mainly as single cells (Suppl.Fig. 3B). No spheroid formation was observed for the MDA-MB-231 cells which were evenly distributed as single cells throughout the hydrogel (Suppl.Fig. 3C). In contrast, MDA-MB-231BO cells formed grape-like loose cell clusters of difference sizes upon 3D culture (Suppl.Fig. 3D).

3.4. Implantation of invasive breast cancer cells using a hydrogel carrier system led to tumour growth *in vivo*

Cell-loaded hydrogels were implanted into the flanks of female NOD/SCID mice in a second surgical procedure after 8 weeks post-implantation of the pre-seeded mPCL-CaP scaffolds (Suppl.Fig. 3E-F). Scaffolds and the cell-loaded hydrogels were fully integrated into the murine soft tissue and were well-vascularised (Suppl.Fig. 3G-H). Initial tumour growth was observed 2 weeks post-implantation of MDA-MB-231 and MDA-MB-231BO cells reaching a terminal volume of 1 cm^3 after 4 weeks. No tumour growth was seen for SUM1315 cells after 4 weeks post-implantation which might be due to their slow growth rate (Kuperwasser *et al.* 2005). As expected, non-malignant MCF10A did not form tumours. The human origin of the osteoblasts and other human cellular and matrix components, present in the mPCL-CaP scaffold (Fig. 4A), was demonstrated by immunohistochemical staining with human-specific antibodies directed against nuclear mitotic apparatus protein (hs-NuMA; Fig. 4B-C), osteocalcin (hs-OC; Fig. 4D), collagen type-I (hs-Col-I; Fig. 4E) and von Willebrand Factor (hs-vWF; Fig. 4E).

3.5. Development of the organ bone and enhanced osteoclastic activity upon presence of highly metastatic breast cancer cells

To explore the crosstalk between breast tumours and the TEBCs, µ-CT and histological analyses were performed 12 weeks post-implantation of the hOB-seeded mPCL-CaP scaffolds and 4 weeks post-implantation of cell-loaded hydrogels. Micro-CT analysis revealed a high ratio of mineralised tissue (average 21 ± 4%) in all groups (Fig. 5A, E, I, M). The BV/TV ratio did not significantly change in any of the malignant cell groups (SUM1315: 0.022 ± 0.013; MDA-MB-231: 0.092 ± 0.041; MDA-MB-231BO: 0.040 ± 0.005) compared to the non-malignant control group (MCF10A: 0.034 ± 0.017; Fig.6A), thus indicating no major changes in the cancer cell-induced osteolysis. There was a significantly lower BC/TV in the SUM1315 tumour group compared to the MDA-MB-231BO tumour group ($P<0.05$). Calcified

areas were also detected in the MDA-MB-231 (Fig. 5I) and MDA-MB-231BO (Fig. 5M) tumours. H&E staining revealed residual PCL in all groups and indicated different tissue types, including new bone (NB), bone marrow (BM), fibrous connective tissue (CT) and tumour tissue (T), with clear blood vessel formation (Fig. 5B-C, F-G, J-K, N-O). New bone formation was detected in the scaffold area and in the hollow parts of the scaffold, where hOBs in addition to rhBMP-7 had been administered. TRAP staining (Fig. 5D, H, L, P; Fig. 3H) indicated a significant increased number of TRAP-positive cells for SUM1315 (0.52 ± 0.11 mm^{-1}), MDA-MB-231 (0.53 ± 0.08 mm^{-1}) and MDA-MB-231-BO (0.41 ± 0.02 mm^{-1}) tumours and the scaffold only (0.26 ± 0.01 mm^{-1}) at the bone interface compared to the non-malignant MCF10A cells (0.03 ± 0.02 mm^{-1}; $P<0.05$; Fig. 6B). The number of TRAP-positive cells and the BV/TV ratio were the highest in the MDA-MB-231 tumour group. MDA-MB-231-BO cells formed significantly bigger tumours (272.3 ± 53.8 mm^3; $P<0.05$) compared to SUM1315 cells (37.75 ± 16.0 mm^3), while MDA-MB-231 cells had medium-sized tumours (88.8 ± 33.4 mm^3; Fig. 6C).

4. Discussion

The development of breast cancer-related bone metastases is a highly dynamic and complex process, which can be mimicked in an *in vivo* disease model consisting of the two main components – a humanised breast tumour and a humanised organ bone. To achieve sufficient bone formation through TE strategies, the first-generation FDA-approved mPCL scaffold was combined with bone marrow-derived stromal cells that had to be immobilised onto the scaffold using fibrin sealant because of its poor protein and cell adhesive properties. To circumvent this approach, a second-generation composite scaffold made from mPCL and TCP was established by fused deposition modelling (Zhou *et al.* 2007). The advantages of composite scaffolds are their improved biomechanical and degradation properties, increased strength via the ceramic phase, toughness and plasticity via the polymer phase (Hutmacher and Cool 2007). These improvements have resulted in advanced cell seeding, adhesion, control and/or incorporation of biological factors like BMPs (Rai *et al.* 2005). In this study, a high seeding efficiency 8 hrs after administration of hOBs onto the mPCL-TCP scaffold was achieved (data not shown).

Porcine bone marrow-derived stromal cells in conjunction with mPCL-TCP scaffolds were used in a subcutaneous rat model, showing sufficient bone formation (Zhou *et al.* 2007). Bone regenerative applications using mPCL-TCP scaffolds, which was loaded with collagen-type I and rhBMP-2, demonstrated a full closure of a critical-sized rat calvarial defect 15 weeks post-implantation (Sawyer *et al.* 2009). Neither short-term nor long-term foreign body

reactions were detectable underscoring the high immunocompatibility of mPCL (Sawyer *et al.* 2009). In this study, osteogenic progenitor cells and rhBMP-7 were used to further increase the osteoinductivity and biological activity of the mPCL-TCP scaffolds, but with mixed results (scaffold 1). The major differences between this study and the aforementioned studies were the subcutaneous localisation of the scaffold and the cell type used. Our group has already shown that ovine osteoblasts grown on mPCL-TCP scaffolds and addition of rhBMP-7 resulted in a sufficient amount of bone (Reichert *et al.* 2011), but yet was not able to achieve similar results in the present study using human osteogenic progenitor cells. One reason might be the mechanical properties of the scaffold as they are favourable for bone TE in orthotopic defect models but can present pitfalls in humanised subcutaneous NOD/SCID mice models.

Hence, it was sought to find a suitable scaffold to engineer a humanised bone microenvironment and upon this to develop an *in vivo* disease model to investigate cancer-related metastasis to this human bone equivalent. Therefore, a bone TE approach for the *in vitro* culture of hOBs was combined with the *in vitro* 3D culture of non-malignant and malignant breast cells within PEG-based hydrogels. Upon implantation of the TEBCs (scaffold 2), a complex organ bone composed of human and murine elements was formed. In addition, the implantation of cell-loaded hydrogels acted as delivery system of human non-malignant and malignant breast cells in NOD/SCID mice.

The mechanical properties are critical for the treatment of bone defects, where an intrinsic stability of the scaffold is desired, but were causing complication in the ectopic side in the NOD/SCID model. The delicate skin of NOD/SCID mice was not strong enough to aid the integration of the scaffold into the soft tissue of the murine flanks to the same extent as reported for the ectopic bone formation in a rat model (Zhou *et al.* 2007). This incomplete integration might be responsible for the apparent gradient in bone formation from the skin towards the muscle. Thus, a mPCL-CaP scaffold (scaffold 2) was chosen for the breast cancer-related metastasis experiments (Kolambkar *et al.* 2010) (Kolambkar *et al.* 2011). The major differences between both scaffolds are the fabrication technique, fused deposition modelling versus solution electrospinning, and the scaffold design, cylindrical versus tubular. In line with a previous study (Kolambkar *et al.* 2010), hOBs formed a dense cell sheet when grown on the perforated mPCL-CaP scaffold and remained viable over 4 weeks *in vitro*. Bone TE properties of these scaffolds were successfully established in a rat femoral defect model, in which scaffolds were combined with rhBMP-2 via an alginate hydrogel, leading to new bone formation and bridging the defect within 12 weeks post-implantation (Kolambkar *et al.* 2011). In the presented study, the orthotopic approach (Kolambkar *et al.* 2011) was

translated to an ectopic setting by improving its bioactivity. The addition of CaP coating, hOBs, which have been osteogenically stimulated pre-implantation, and rhBMP-7 resulted in a humanised organ bone at an ectopic site in NOD/SCID mice, allowing the study of cancer-related bone metastasis.

Only few groups use a bone TE approach to study the mechanisms of bone metastasis in ectopic NOD/SCID models. Moreau *et al*. (Moreau *et al.* 2007) utilised a biodegradable silk scaffold together with human mesenchymal stem cells (hMSCs) and rhBMP-2. Development of matured bone occurred 7 weeks after *in vitro* culture under osteogenic conditions, but did not mediate breast cancer cell colonisation (Moreau *et al.* 2007). Instead, the more primitive bone microenvironment resulted in a higher amount of breast cancer cell colonisation 3 months post-implantation at its orthotopic site, the mammary fat pad. The application of this silk scaffold combined with either hMSC or rhBMP-2 had the highest effect on metastatic spread compared to their combination (Moreau *et al.* 2007). This suggests breast cancer cells homed towards hMSCs grown on the silk scaffold rather than towards the tissue-engineered bone construct (Moreau *et al.* 2007). The presented TE approach herein utilised hOBs in addition to rhBMP-7 in fibrin sealant and aimed for the generation of mature human bone as target tissue for breast cancer cell colonisation. Thus, it is of utmost importance to represent all elements of the organ bone in an ectopic bone assay that includes mineralised tissue, osteoblasts, osteocytes, osteoclasts and bone marrow. Several other studies have shown that TE approaches lead to mineralised tissue formation in ectopic bone models, but without the development of bone marrow (Kuperwasser *et al.* 2005) (Moreau *et al.* 2007) (Roldan *et al.* 2010).

Our bone TE approach indicated that the newly formed bone is of human origin. Immunohistochemical analysis indicated the presence of matrix-embedded osteocytes of human origin as well as human-derived osteocalcin and collagen type-I in the TEBCs. The appearance of human spindle-shaped cells in the connective and cartilaginous tissues suggests that the implanted hOBs and not the murine cells mainly participated in the endochondral bone formation. The human-derived bone-specific matrix proteins osteocalcin and collagen type-I were mostly located in the center of the organ bone, demonstrating that the outer cortical-like shell surrounding the scaffold is a chimera of both human and murine extracellular matrix. This finding is consistent with our previous approach (Thibaudeau *et al.* 2014a) (Thibaudeau *et al.* 2014b). To date, several groups ulilised approaches, such as Matrigel or fibrin gels, other than tissue-engineered bone constructs to humanise the bone marrow microenvironment to study for example normal and malignant hematopoiesis (Sacchetti *et al.* 2007) (Chen *et al.* 2012) (Reinisch *et al.* 2016). 3D bioprinting can be used to generate a biomimetic bone matrix that consists of gelatine-based hydrogels loaded with

human osteoblasts or human bone marrow-derived MSCs to study their functional interaction with breast cancer cells (Zhou *et al.* 2016).

A well-established hydrogel model was used to deliver human breast cancer cells. Evidently, 3D cell culture platforms mimic physiological cellular microenvironment, mimicking the natural cellular behaviour compared to 2D cultures on tissue culture plastic. Our group established PEG-based hydrogels as 3D platform for human ovarian cancer cells (Loessner *et al.* 2010). These synthetically-derived biomaterials are well-defined opposed to other commonly-used biomaterials in the cancer research, like Matrigel, which harbour high batch-to-batch variations that complicate data analysis (Loessner *et al.* 2010). To examine the integral step of the metastatic cascade, the bone colonisation by breast cancer cells, PEG-based hydrogels were used to implant breast cancer cells adjacent to the TEBCs. Tumour formation was observed within 4 weeks post-implantation. Macroscopic analysis upon explantation showed sufficient vascularisation of the tumours and the TEBCs as well as blood vessels shared by both. A significantly higher number of osteoclasts were found in the TEBCs in conjunction with the invasive breast cancer cells compared to the control. These findings indicate reciprocal interactions between the tumour and TEBCs. However, future experiments need to be performed to further confirm these interactions.

The majority of ectopic bone models utilise human bone chips (Kuperwasser *et al.* 2005) or silk scaffolds seeded with hMSCs (Moreau *et al.* 2007) that are implanted into immune-suppressed animals. While the implanted human bone chips are often poorly vascularised and have a high dehiscence rate, in turn, previous bone TE approaches often failed to produce sufficient bone volume to allow the analysis of reciprocal interactions with breast cancer cells. In this study, a notably large bone volume in NOD/SCID mice was engineered. Strikingly, this bone comprises hallmarks of the organ bone, such as bone marrow, reticular and adipocytic stroma, hematopoietic cells, bone-lining osteoblasts and osteoclasts. This *in vivo* disease model significantly increased osteoclast recruitment, thus recapitulating clinically relevant osteolytic lesions. It should be noted that this humanised model using a subcutaneous approach in NOD/SCID mice still harbours features of both species, human and murine. As NOD/SCID mice are hosting the human TEBCs, it is assumed that the vascularisation, osteoclasts and the bone marrow are provided by the murine host. Our group has shown that osteoblasts remained at the implantations site within the mineralized matrix when using ovine osteoblasts instead of hOBs in conjunction with rhBMP-7 and the identical mPCL-TCP scaffold (Reichert *et al.* 2011). Hence, it is assumed that hOBs also

remain within their bone-like matrix deposited onto the scaffold, thus providing a humanised organ bone within the murine host.

Acknowledgements

The authors like to acknowledge the Queensland University of Technology, the Australian Research Council (ARC) and the German Academic Exchange Service (DAAD) for funding and Olympus Biotech for supplying the rhBMP-7. We thank Dr Christina Theodoropoulos and Dr Ferdinand Wagner for proof reading the manuscript and assistance with the immunohistochemistry.

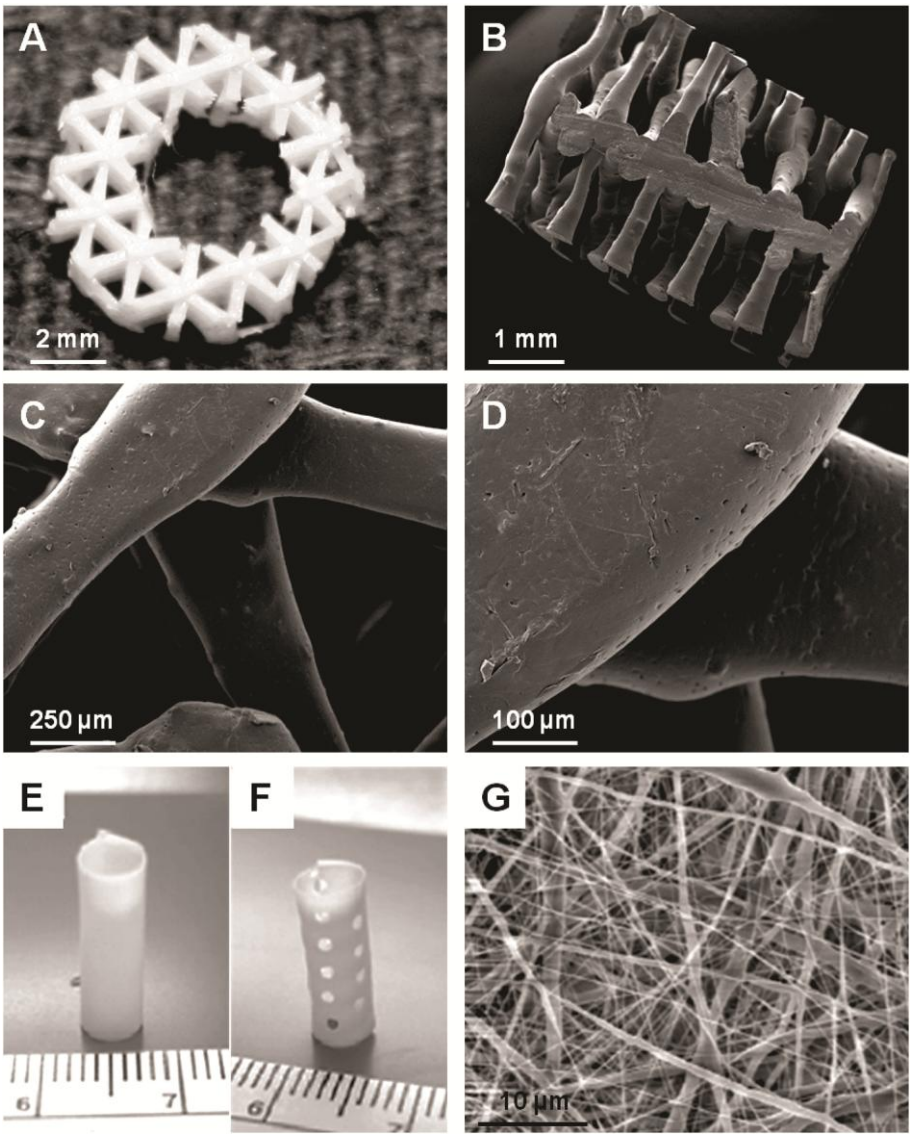

Figure 1. A. Cylindrical mPCL-TCP scaffold produced by fused deposition modelling (scaffold 1). B-D. Scanning electron micrographs of mPCL-TCP scaffold. E-F. Tubular mPCL-CaP scaffold produced by solution electrospinning (scaffold 2); image reproduced from (Kolambkar *et al.* 2011). G. Scanning electron micrograph of mPCL-CaP scaffold sheets prior to tubular shaping, with random non-woven fibres and a broad range fibre diameter (51-974 nm); image reproduced from (Kolambkar *et al.* 2011).

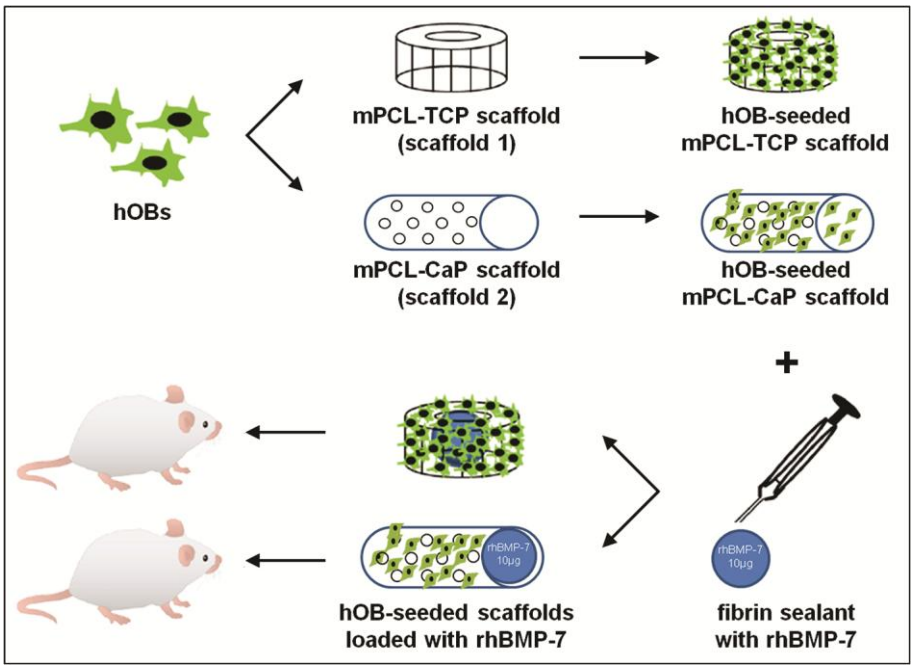

Figure 2. Primary human osteoblasts (hOBs) were seeded onto mPCL-TCP and mPCL-CaP scaffolds in osteogenic culture conditions. After 4 weeks, hOB-seeded scaffolds were combined with rhBMP-7-containing fibrin sealant and implanted into the flanks of NOD/SCID mice subcunateously. After 12 weeks, scaffolds were explanted for subsequent analyses.

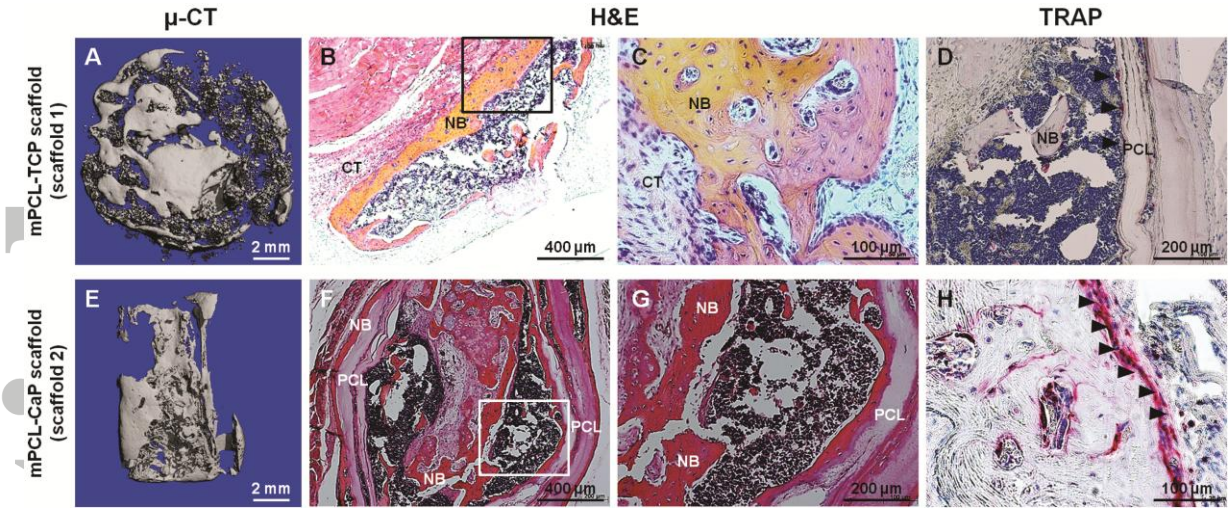

Figure 3. A, E. Micro-CT images showing scattered mineralised tissue in the mPCL-TCP scaffold and equally distributed mineralised tissue in the mPCL-CaP scaffold. B-C, F-G. H&E staining demonstrate new bone formation in both scaffolds (squared boxes represent areas if higher magnification shown in C, G; NB, new bone; CT, connective tissue; PCL, polycaprolactone); images shown in A-D reproduced from (Quent *et al.* 2016). D, H. TRAP staining reveals osteoclastic activity in both scaffolds, with more TRAP-positive cells in the mPCL-CaP scaffold (black arrows; NB, new bone; PCL, polycaprolactone).

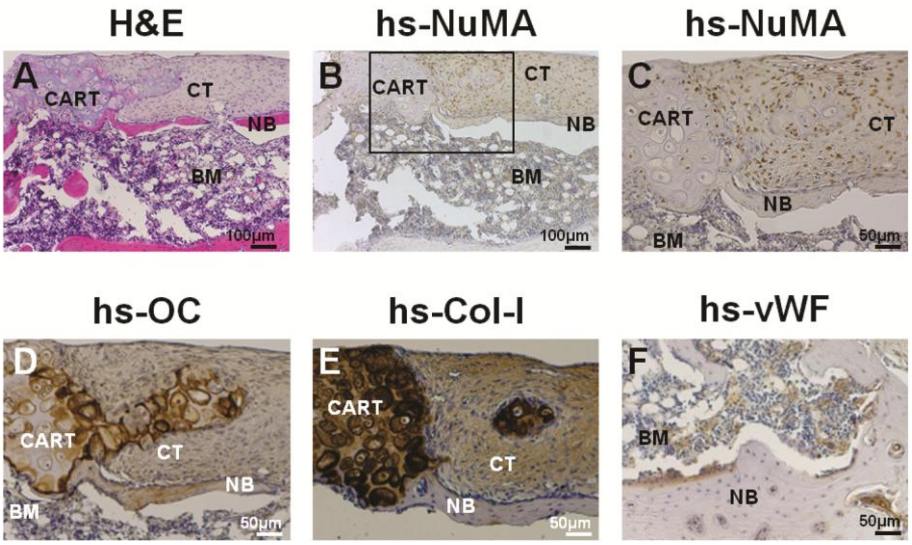

Figure 4. A. H&E staining of the mPCL-CaP scaffold confirmed new bone and bone marrow formation. B-C. Human-derived osteoblasts are indicated by positive staining for nuclear mitotic apparatus protein (hs-NuMA; squared box represents area if higher magnification shown in C). D-E. The presence of bone-specific matrix proteins is detected by human-specific antibodies against osteocalcin (hs-OC) and collagen type-I (hs-Col-I). F. Other human-derived factors within the bone and bone marrow compartment are indicated by positive staining for human-specific von Willebrand Factor (hs-vWF; NB, new bone; BM, bone marrow; CT, connective tissue; CART, cartilage).

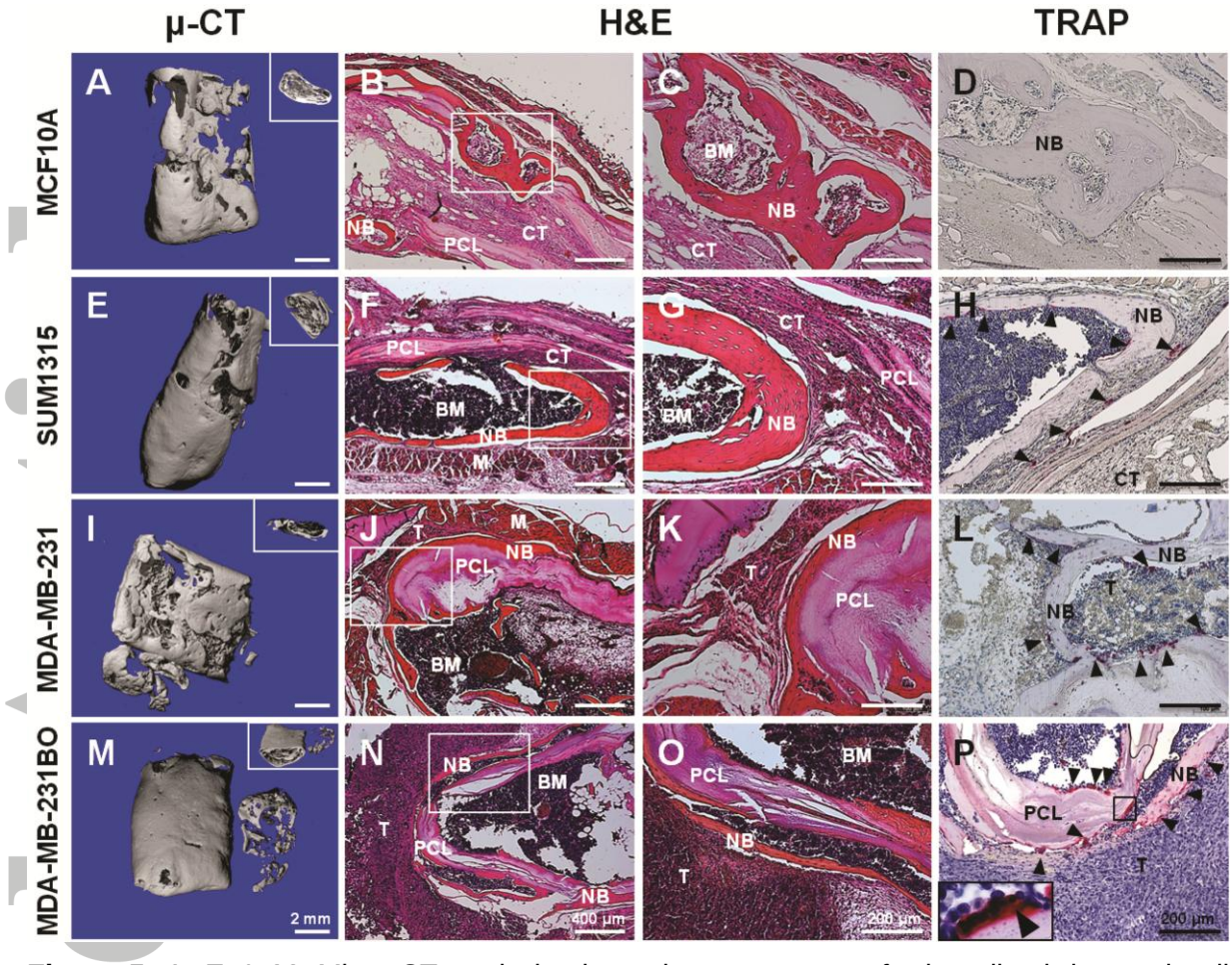

Figure 5. A, E, I, M. Micro-CT analysis shows large amounts of mineralised tissues in all experimental groups (inserts represent cross-sections). B-C, F-G, J-K, N-O. H&E staining correlates with the mineralised tissue detected by µ-CT and indicates new bone formation, tumour and connective tissues and the presence of bone marrow (squared boxes represent areas if higher magnification shown in C, G, K, O; NB, new bone; CT, connective tissue; PCL, polycaprolactone; BM, bone marrow; M, murine muscle; T, tumor tissue). D, H, L, P. TRAP staining is apparent in SUM1315, MDA-MB-231 and MDA-MB-231BO groups (black arrows; squared box represent area if higher magnification shown in the insert), while no TRAP-positive cells are present in the non-malignant MCF10A group (NB, new bone; CT, connective tissue; PCL, polycaprolactone; T, tumor tissue).

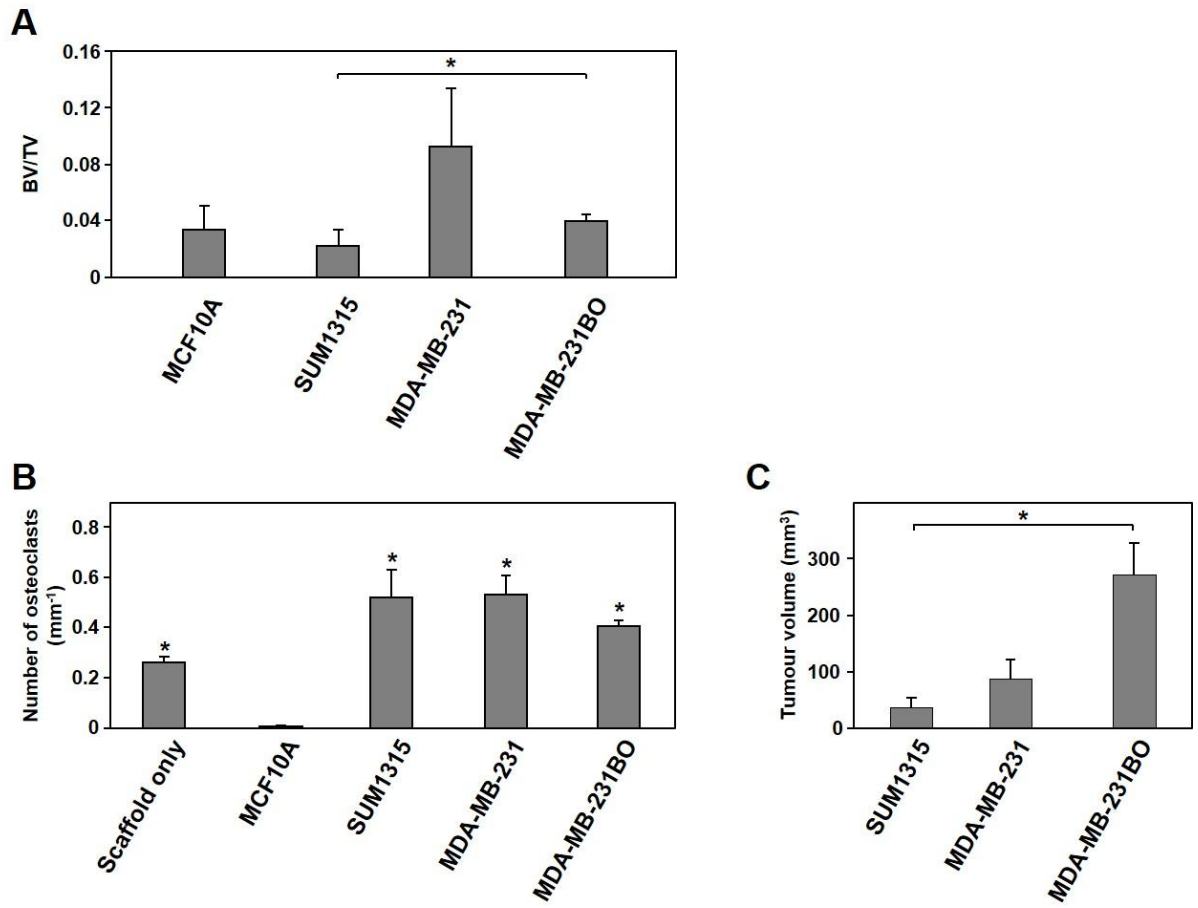

Figure 6. A. BV/TV did not significantly change in any of the tumour groups compared to the non-malignant control. BC/TV was significantly decreased in the SUM1315 tumour group compared to the MDA-MB-231BO tumour group (n=3, mean ± SEM, ***** P<0.05). B. Number of osteoclasts found on the bone interface was significantly increased in the scaffold only group and in the presence of SUM1315, MDA-MB-231 and MDA-MB-231BO cells compared to the non-malignant MCF-10 cells (n=3, mean ± SEM, ***** P<0.05). C. Tumour volume was calculated using the tumour dimensions measured with a vernier calliper; non-malignant MCF-10 cells did not form any tumours (n=3, mean ± SEM, ***** P<0.05).

References

Arthur A, Zannettino A, Gronthos S. 2009, The therapeutic applications of multipotential mesenchymal/stromal stem cells in skeletal tissue repair, *J Cell Physiol*, **218**: 237-245.

Bersani F, Lee J, Yu M, Morris R, Desai R, Ramaswamy S, Toner M, Haber DA, Parekkadan B. 2014, Bioengineered implantable scaffolds as a tool to study stromal-derived factors in metastatic cancer models, *Cancer Res*, **74**: 7229-7238.

Biggs MJ, Richards RG, Gadegaard N, Wilkinson CD, Oreffo RO, Dalby MJ. 2009, The use of nanoscale topography to modulate the dynamics of adhesion formation in primary osteoblasts and ERK/MAPK signalling in STRO-1^+ enriched skeletal stem cells, *Biomaterials*, **30**: 5094-5103.

Brown JE, Neville-Webbe H, Coleman RE. 2004, The role of bisphosphonates in breast and prostate cancers, *Endocr Relat Cancer*, **11**: 207-224.

Chen Y, et al. 2012, Human extramedullary bone marrow in mice: a novel in vivo model of genetically controlled hematopoietic microenvironment, *Blood*, **119**: 4971-4980.

Coleman MP, et al. 2008, Cancer survival in five continents: a worldwide population-based study (CONCORD), *Lancet Oncol,* **9**: 730-756.

Coleman RE, Rubens RD. 1987, The clinical course of bone metastases from breast cancer, *Br J Cancer*, **55**: 61-66.

Daniele G, et al. 2011, Anticancer effect of bisphosphonates: new insights from clinical trials and preclinical evidence, *Expert Rev Anticancer Ther*, **11**: 299-307.

DeSantis C, Siegel R, Bandi P, Jemal A. 2011, Breast cancer statistics, 2011, *CA Cancer J Clin*, **61**: 409-418.

Hutmacher DW. 2000, Scaffolds in tissue engineering bone and cartilage, *Biomaterials*, **21**: 2529-2543.

Hutmacher DW, Cool S. 2007, Concepts of scaffold-based tissue engineering--the rationale to use solid free-form fabrication techniques, *J Cell Mol Med*, **11**: 654-669.

Kang Y, Siegel PM, Shu W, Drobnjak M, Kakonen SM, Cordon-Cardo C, Guise TA, Massague J. 2003, A multigenic program mediating breast cancer metastasis to bone, *Cancer Cell*, **3**: 537-549.

Khanna C, Hunter K. 2005, Modeling metastasis in vivo, *Carcinogenesis*, **26**: 513-523.

Kolambkar YM, Peister A, Ekaputra AK, Hutmacher DW, Guldberg RE. 2010, Colonization and osteogenic differentiation of different stem cell sources on electrospun nanofiber meshes, *Tissue Eng Part A*, **16**: 3219-3230.

Kolambkar YM, Dupont KM, Boerckel JD, Huebsch N, Mooney DJ, Hutmacher DW, Guldberg RE. 2011, An alginate-based hybrid system for growth factor delivery in the functional repair of large bone defects, *Biomaterials*, **32**: 65-74.

Kozlow W, Guise TA. 2005, Breast cancer metastasis to bone: mechanisms of osteolysis and implications for therapy, *J Mammary Gland Biol Neoplasia*, **10**: 169-180.

Kuperwasser C, Dessain S, Bierbaum BE, Garnet D, Sperandio K, Gauvin GP, Naber SP, Weinberg RA, Rosenblatt M. 2005, A mouse model of human breast cancer metastasis to human bone, *Cancer Res*, **65**: 6130-6138.

Lau WM, Doucet M, Stadel R, Huang D, Weber KL, Kominsky SL. 2013, Enpp1: a potential facilitator of breast cancer bone metastasis, *PLoS One*, **8**: e66752.

Loessner D, Stok KS, Lutolf MP, Hutmacher DW, Clements JA, Rizzi SC. 2010, Bioengineered 3D platform to explore cell-ECM interactions and drug resistance of epithelial ovarian cancer cells, *Biomaterials*, **31**: 8494-8506.

Moreau JE, Anderson K, Mauney JR, Nguyen T, Kaplan DL, Rosenblatt M. 2007, Tissue-engineered bone serves as a target for metastasis of human breast cancer in a mouse model, *Cancer Res*, **67**: 10304-10308.

Psaila B, Kaplan RN, Port ER, Lyden D. 2006, Priming the 'soil' for breast cancer metastasis: the pre-metastatic niche, *Breast Dis*, **26**: 65-74.

Quent VM, Theodoropoulos C, Hutmacher DW, Reichert JC. 2016, Differential osteogenicity of multiple donor-derived human mesenchymal stem cells and osteoblasts in monolayer, scaffold-based 3D culture and in vivo, *Biomed Tech* (Berl), **61**: 253-266.

Rai B, Teoh SH, Hutmacher DW, Cao T, Ho KH. 2005, Novel PCL-based honeycomb scaffolds as drug delivery systems for rhBMP-2, *Biomaterials*, **26**: 3739-3748.

Reichert JC, Quent VM, Noth U, Hutmacher DW. 2011, Ovine cortical osteoblasts outperform bone marrow cells in an ectopic bone assay, *J Tissue Eng Regen Med*, **5**: 831-844.

Reinisch A, et al. 2016, A humanized bone marrow ossicle xenotransplantation model enables improved engraftment of healthy and leukemic human hematopoietic cells, *Nat Med*, **22**: 812-821.

Roldan JC, Detsch R, Schaefer S, Chang E, Kelantan M, Waiss W, Reichert TE, Gurtner GC, Deisinger U. 2010, Bone formation and degradation of a highly porous biphasic calcium phosphate ceramic in presence of BMP-7, VEGF and mesenchymal stem cells in an ectopic mouse model, *J Craniomaxillofac Sur*, **38**: 423-430.

Sacchetti B, et al. 2007, Self-renewing osteoprogenitors in bone marrow sinusoids can organize a hematopoietic microenvironment, *Cell* **131**: 324-336.

Santos MI, Unger RE, Sousa RA, Reis RL, Kirkpatrick CJ. 2009, Crosstalk between osteoblasts and endothelial cells co-cultured on a polycaprolactone-starch scaffold and the in vitro development of vascularization, *Biomaterials*, **30**: 4407-4415.

Sawyer AA, Song SJ, Susanto E, Chuan P, Lam CX, Woodruff MA, Hutmacher DW, Cool SM. 2009, The stimulation of healing within a rat calvarial defect by mPCL-TCP/collagen scaffolds loaded with rhBMP-2, *Biomaterials*, **30**: 2479-2488.

Schuster J, Zhang J, Longo M. 2006, A novel human osteoblast-derived severe combined immunodeficiency mouse model of bone metastasis, *J Neurosurg Spine*, **4**: 388-391.

Seib FP, Berry JE, Shiozawa Y, Taichman RS, Kaplan DL. 2015, Tissue engineering a surrogate niche for metastatic cancer cells, *Biomaterials*, **51**: 313-319.

Thibaudeau L, Quent VM, Holzapfel BM, Taubenberger AV, Straub M, Hutmacher DW. 2014a, Mimicking breast cancer-induced bone metastasis in vivo: current transplantation models and advanced humanized strategies, *Cancer Metastasis Rev*, **33**: 721-735.

Thibaudeau L, et al. 2014b, A tissue-engineered humanized xenograft model of human breast cancer metastasis to bone, *Dis Model Mech*, **7**: 299-309.

Vaquette C, Ivanovski S, Hamlet SM, Hutmacher DW. 2013, Effect of culture conditions and calcium phosphate coating on ectopic bone formation, *Biomaterials*, **34**: 5538-5551.

Xia TS, et al. 2012, Bone metastasis in a novel breast cancer mouse model containing human breast and human bone, *Breast Cancer Res Treat*, **132**: 471-486.

Yang F, Wolke JGC, Jansen JA. 2008, Biomimetic calcium phosphate coating on electrospun poly (epsilon-caprolactone) scaffolds for bone tissue engineering, *Chem Eng J,* **137**: 154-161.

Yonou H, Yokose T, Kamijo T, Kanomata N, Hasebe T, Nagai K, Hatano T, Ogawa Y, Ochiai A. 2001, Establishment of a novel species- and tissue-specific metastasis model of human prostate cancer in humanized non-obese diabetic/severe combined immunodeficient mice engrafted with human adult lung and bone, *Cancer Res*, **61**: 2177-2182.

Yu HH, Tsai YY, Hoffe SE. 2012, Overview of diagnosis and management of metastatic disease to bone, *Cancer Control*, **19**: 84-91.

Zhou Y, Chen F, Ho ST, Woodruff MA, Lim TM, Hutmacher DW. 2007, Combined marrow stromal cell-sheet techniques and high-strength biodegradable composite scaffolds for engineered functional bone grafts, *Biomaterials*, **28**: 814-824.

Zhou X, Zhu W, Nowicki M, Miao S, Cui H, Holmes B, Glazer RI, Zhang LG. 2016, 3D Bioprinting a cell-laden bone matrix for breast cancer metastasis study. *ACS Appl Mater Interfaces*, **8**: 30017-30026.

Table 1. List of antibodies used for immunohistochemistry.

Antibody	Name	Company	Cat.No.	Host species	Dilution
NuMA	Nuclear mitotic apparatus protein	Epitomics	S2825	rabbit, polyclonal	1:100
OC	Osteocalcin	Abcam	ab13418, #OC4-30	mouse, monoclonal	1:200
Col-I	Collagen type-I	MP Biomedicals	63170, #I-8H5	mouse, monoclonal	1:300
vWF	von Willebrand Factor	Merck Millipore	ab7356	rabbit, polyclonal	1:300